A&A 368, 994–1005 (2001)
DOI: 10.1051/0004-6361:20010068

Astronomy & Astrophysics

Physical parameters of sdB stars from spectral energy distributions⋆

R. Aznar Cuadrado and C. S. Jeffery

Armagh Observatory, College Hill, Armagh BT61 9DG, N. Ireland
e-mail: csj@star.arm.ac.uk

Received 21 July 2000 / Accepted 4 January 2001

Abstract. The atmospheric parameters of 34 hot subdwarf B stars have been obtained using a combination of 61 short and long-wave IUE spectra, together with new and existing optical and infrared photometric data. Using a grid of high-gravity helium-deficient model atmospheres and a χ^2-minimization procedure, 15 single sdB stars and 19 composite systems, containing a hot subdwarf B star and a cool main-sequence companion, were analyzed. From the ($\log L$–$\log T_{\rm eff}$) diagram of our results, we conclude that the majority of the cool companions to our sample of binary sdB stars are main sequence stars, in the range of $4000 < T_{\rm eff}/\,{\rm K} < 6000$ and mass $0.8 < M/M_{\odot} < 1.3$. The lower limit on detectability of cool stars in composite sdB of our sample is ∼3600 K, corresponding to a spectral type of M1 or later (Lang 1992).

Key words. stars: formation, early-type, subdwarfs, fundamental parameters (luminosities, temperatures) – binaries: spectroscopic

1. Introduction

Subdwarf B (sdB) stars are considered to be core helium burning stars of mass ∼0.5 $M_{\odot}$ with a very thin hydrogen-rich envelope ($\lesssim$0.01 $M_{\odot}$, Heber 1986). However, their evolutionary status it is still unclear. It is very difficult to account for the very small hydrogen envelope mass within single-star evolution theory (Sweigart 1997). The hypothesis of close binary evolution was firstly suggested by Mengel et al. (1976) to explain the formation of sdB stars, and latterly corroborated by Saffer et al. (1998) with the discovery of short-period systems of white dwarfs and sdB stars. Hence, it is important to investigate whether binary star interactions can explain the removal of surface hydrogen.

Excess infrared flux from the direction of a hot subdwarf star can be interpreted in several ways. It can be due to a late type companion, hot dust surrounding the star, or free-free emission from a stellar wind. In each case the data can be analysed to yield information on the hot subdwarf and its evolution.

Previous studies have indicated that many sdB stars are members of binary systems with cool companions (e.g. Allard et al. 1994), fractions of between 50% and 100% have been claimed (Bixler et al. 1991). The point in studying companions to hot subdwarfs is that we can learn things about the hot subdwarfs that are not easy to observe directly due to the problems of modelling hot atmospheres and the relatively large distances to these stars that, currently, preclude astrometric analysis for the majority.

Another interest lies in the classification of the secondary stars, as this information can be used to set limits on how the hot subdwarfs formed. Deconvolving the energy distribution of the detectable binary sdB stars of our sample, would permit an estimate of the position of the secondaries within the HR diagram, a question of persistent interest for stellar evolution studies.

In this work, we make an attempt to determine the atmospheric parameters of a sample of 34 hot subdwarf B stars. UV, optical and infrared fluxes are interpreted with the aid of high-gravity hydrogen-rich model atmospheres and a χ^2-minimization procedure. In Sect. 2 the observations and data calibration are described. In Sect. 3 existing ultraviolet spectra and optical and infrared data are presented, together with new Strömgren *uvby* and near–infrared Johnson *RI* photometry of a small sample of hot subdwarf B stars. In Sect. 4 the procedure used to fit the observations and determine the atmospheric parameters is described. Section 5 presents the resulting atmospheric parameters of our sample of 34 sdB stars, along with an internal error analysis. The results presented are compared in Sect. 6 with those in the literature, including previous determinations of the atmospheric parameters.

Send offprint requests to: R. Aznar Cuadrado,
e-mail: rea@star.arm.ac.uk

⋆ Based on observations made with the Jacobus Kapteyn Telescope operated on the island of La Palma by the Isaac Newton Group in the Spanish Observatorio del Roque de los Muchachos of the Instituto de Astrofísica de Canarias, and on INES data obtained with the IUE satellite.

In Sect. 7 the Hertzsprung-Russell diagram of the sample is discussed. A discussion and conclusions are presented in Sects. 8 and 9, respectively.

2. Optical and near–infrared observations and data calibration

Strömgren *uvby* and Johnson *RI* photometry was obtained in two different observing runs during the nights of 1999, June 1, 2, 3, and in 2000, May 10, with the 1.0 m Jacobus Kapteyn Telescope (JKT), at the Isaac Newton Group of Telescopes, La Palma. The detectors used in those runs were the 1024 × 1024 TEK4 and the 2K × 2K SITe2 CCD, respectively. Standard aperture photometry was performed on a sample of 13 hot subdwarfs.

Secondary Strömgren standards from Stetson (1991) observed in *uvb* and *y* filters and Johnson standards from Landolt (1992) observed in *R* and *I* filters were used to derive the instrumental colour transformations and extinction coefficients. Standards were observed close to the zenith during evening and morning twilight, and at regular intervals throughout each night. Bias exposures were taken each afternoon and sky flat-field frames were obtained in each twilight. Several observations of each sdB star were made in each filter in order to improve photometric accuracy.

For a determination of the instrumental colour transformation of the standard system, extinction coefficients and zero points, initial CCD reduction was carried out using the standard data reduction package IRAF/CCDRED (Massey 1992). This included the trimming of the data section, bias and flat-field corrections. Instrumental magnitudes for the standard stars were determined using aperture photometry techniques within the IRAF package DAOPHOT (Massey & Davies 1992). An aperture of radius 14″ was chosen in order to be consistent when calibrating the instrumental magnitudes of our standard stars with results obtained by Landolt (1991) and Stetson (1992).

Colour-dependent transformations were applied to determine standard magnitudes from our instrumental magnitudes. The transformation equations were solved using tasks within the IRAF package PHOTCAL (Massey & Davies 1992).

From the sample of stars observed during these two observing runs, 13 sdB stars, the fraction which is contaminated by unrelated background/foreground stars is small (15%), where the nearest stars in the field is found within 10 arcsec from our target (Thejll et al. 1994). A faint star has been observed close to *PG 1230+052* and *PG 1452+198*.

3. Archival UV, optical and infrared data

In order to complement our Strömgren *uvby* and Johnson *RI* photometry of a sample of hot subdwarf stars, and to be able to perform our energy distribution analysis, we have compiled published optical and infrared data, as well as ultraviolet data from the IUE (*International Ultraviolet Explorer*) satellite.

Table 1. Table of large-aperture IUE spectra used in this work. "LWP", "LWR" and "SWP" respectively indicate spectra taken with the Long Wavelength Prime, Long Wavelength Redundant and Short Wavelength Prime cameras. "R" after SPW files indicates high resolution 1D spectra, rebinned onto low resolution wavelength scale

	Object	LW Image	exp(s)	SW Image	exp(s)
1	PG 0004+133	LWP18429	1080	SWP39286	960
2	PG 0105+276			SWP56271	1500
3	PG 0110+262			SWP55828	600
4	PG 0229+064			SWP48617R	22320
5	PG 0232+095	LWP18430	420	SWP39287	360
				SWP39288	720
6	PG 0240+046	LWP18452	2700	SWP39307	2100
7	PG 0314+146			SWP51740	600
8	PG 0342+026	LWP07462	160	SWP27466R	9600
9	PG 0749+658	LWP31669	180	SWP56166	300
10	PG 0839+399	LWP09826	1800	SWP29995	1800
11	PG 0856+121	LWP03484	1200	SWP23159	900
12	PG 0900+400	LWP30587	1200	SWP54558	1200
13	PG 0934+186	LWP07463	2100	SWP27468	1500
		LWP08298	1080	SWP28393	1200
14	PG 1040+234			SWP56384	1200
15	PG 1047+003	LWP08242	1200	SWP28350	900
16	PG 1049+013			SWP57007	3600
17	PG 1104+243	LWP06222	240	SWP27465R	12600
18	PG 1230+052	LWP08243	1260	SWP26176	600
19	PG 1233+426	LWP02149	330	SWP21373R	18000
20	PG 1336 -018	LWP06224	840	SWP26175	1080
21	PG 1432+004	LWP03501	840	SWP23176	600
22	PG 1433+239	LWR03302	840	SWP03722	780
23	PG 1449+653	LWR14118	21840	SWP34298	900
24	PG 1452+198	LWP03503	480	SWP23178	360
25	PG 1629+081	LWP13481	540	SWP33790	420
26	PG 1701+359	LWP21097	1200	SWP42337	1500
27	PG 1718+519	LWP20308	1200	SWP41571	450
28	BD+29° 3070	LWR16266	215	SWP20344	140
29	PG 2110+127			SWP41573	300
30	PG 2135+045			SWP57331	3600
31	PG 2148+095			SWP56148	600
32	PG 2214+184			SWP44816	1200
33	PG 2226+094			SWP56149	1200
34	PG 2259+134	LWP23244	1320	SWP44821	2460
				SWP56182	1500

3.1. IUE observations

61 low-resolution observations of 34 sdB stars made with the large aperture (LAP) of the *International Ultraviolet Explorer* (IUE) have been collected from the IUE Final Archive, as "IUE Newly Extracted Spectra" (INES, Nichols & Linsky 1996), and are shown in Table 1. Column 1 shows the name and an identification number of each star, Cols. 2 and 4 give the sequential image numbers from the Long Wavelength Prime and Redundant (LWP and LWR) and Short Wavelength Prime (SWP) cameras. Columns 3 and 5 show the effective exposure times of each image. An "R" after SWP image number indicates a high resolution spectrum, which has been rebinned onto the low resolution wavelength scale.

3.2. Optical and infrared data

Published optical Johnson-Morgan *UBV* and Strömgren *uvby* data, and infrared Johnson *RIJHK* photometry have

Table 2. Infrared Johnson *RIJHK* photometry of all sdB stars used in this work. Sources: [a] from observations taken with the JKT in June 1999; [b] from Allard et al. (1994); [c] from Ferguson et al. (1984); [d] from Lipunova & Shugarov (1991); [e] from Ulla & Thejll (1998); [f] from Thejll et al. (1995); [g] from observations taken with the JKT in June 2000; [h] from the 2MASS Second Incremental Release Point Source Catalog (Cutri et al. 2000)

	star	R	σ_R	I	σ_I	J	σ_J	H	σ_H	K	σ_K
1	PG 0004+133	13.062[b]	0.008	13.099[b]	0.023	13.301[h]	0.031	13.313[h]	0.033	13.343[h]	0.044
2	PG 0105+276	14.362[b]	0.006	14.349[b]	0.020	14.347[h]	0.043	13.821[h]	0.043	13.712[h]	0.054
3	PG 0110+262	12.892[b]	0.010	12.744[b]	0.012	12.442[h]	0.032	12.222[h]	0.036	12.181[h]	0.029
4	PG 0229+064	11.999[b]	0.025	12.105[b]	0.026	12.290[f]	0.180	12.320[f]	0.150	12.350[f]	0.130
5	PG 0232+095	———	———	———	———	11.090[f]	0.130	10.770[f]	0.070	10.620[f]	0.110
8	PG 0342+026	11.022[b]	0.015	11.092[b]	0.019	11.670[e]	0.080	11.890[e]	0.130	11.860[e]	0.200
9	PG 0749+658	12.100[b]	0.000	12.028[b]	0.000	———	———	———	———	———	———
10	PG 0839+399	14.442[g]	0.005	14.635[g]	0.012	14.850[h]	0.035	15.096[h]	0.068	15.006[h]	0.108
11	PG 0856+121	13.933[g]	0.055	13.073[g]	0.082	13.931[h]	0.038	14.034[h]	0.050	14.137[h]	0.076
12	PG 0900+400	12.570[c]	0.000	12.290[d]	0.000	11.922[h]	0.034	11.616[h]	0.051	11.484[h]	0.036
13	PG 0934+186	13.267[g]	0.009	13.516[g]	0.020	13.751[h]	0.029	13.947[h]	0.043	13.875[h]	0.044
14	PG 1040+234	13.283[b]	0.024	13.107[b]	0.024	12.758[h]	0.029	12.503[h]	0.032	12.448[h]	0.034
15	PG 1047+003	13.489[a]	0.145	13.643[a]	0.151	14.114[h]	0.030	14.210[h]	0.040	14.300[h]	0.077
16	PG 1049+013	14.351[b]	0.000	14.185[b]	0.000	———	———	———	———	———	———
17	PG 1104+243	11.161[b]	0.018	11.001[b]	0.019	10.732[h]	0.031	10.523[h]	0.031	10.451[h]	0.024
18	PG 1230+052	13.355[a]	0.076	13.538[a]	0.074	———	———	———	———	———	———
19	PG 1233+426	12.142[g]	0.002	12.342[g]	0.003	12.630[h]	0.034	12.716[h]	0.032	12.837[h]	0.040
20	PG 1336 -018	13.370[a]	0.194	13.483[a]	0.204	———	———	———	———	———	———
21	PG 1432+004	12.817[a]	0.086	12.965[a]	0.084	———	———	———	———	———	———
22	PG 1433+239	12.654[a]	0.062	12.834[a]	0.061	———	———	———	———	———	———
23	PG 1449+653	13.538[b]	0.000	13.527[b]	0.000	———	———	———	———	———	———
24	PG 1452+198	12.644[g]	0.001	12.848[g]	0.003	13.058[h]	0.032	13.178[h]	0.031	13.273[h]	0.040
25	PG 1629+081	12.774[b]	0.049	12.771[b]	0.051	———	———	———	———	———	———
26	PG 1701+359	13.244[b]	0.053	13.249[b]	0.053	13.140[h]	0.032	12.938[h]	0.032	12.882[h]	0.035
27	PG 1718+519	13.577[b]	0.024	13.395[b]	0.029	13.008[h]	0.026	12.716[h]	0.032	12.664[h]	0.033
28	BD+29° 3070	10.014[a]	0.035	9.979[a]	0.035	9.740[e]	0.010	9.550[e]	0.010	9.540[e]	0.030
29	PG 2110+127	12.758[b]	0.008	12.577[b]	0.011	12.260[e]	0.070	12.070[e]	0.050	12.120[e]	0.080
30	PG 2135+045	14.627[b]	0.022	14.597[b]	0.059	———	———	———	———	———	———
31	PG 2148+095	12.961[b]	0.015	12.865[b]	0.017	12.180[e]	0.110	12.340[e]	0.170	12.060[e]	0.400
32	PG 2214+184	14.205[a]	0.037	14.423[a]	0.037	———	———	———	———	———	———
33	PG 2226+094	13.903[b]	0.012	13.666[b]	0.032	———	———	———	———	———	———
34	PG 2259+134	14.570[a]	0.041	14.808[a]	0.041	14.910[h]	0.042	14.857[h]	0.063	14.897[h]	0.140

been collected as follows. Strömgren *uvby* photometry has been adopted from Wesemael et al. (1992) for all sdB stars used in this work, with the exception of *BD+29° 3070* for which we have used our observations with the JKT (J99): $u = 11.116 \pm 0.299$, $b = 10.383 \pm 0.020$, $v = 10.097 \pm 0.022$, $y = 9.952 \pm 0.025$. Broad band photometry has been adopted for *PG 0900+400*: $U = 12.140$, $B = 13.100$, $V = 12.870$ (Ferguson et al. 1984), and *PG 1433+239*: $U = 11.330$, $B = 12.340$, $V = 12.540$ (Iriarte 1959). Table 2 shows the infrared Johnson *RIJHK* photometric data used in this work, together with their sources.

The photometric magnitudes used in our energy distribution analysis were converted into fluxes using $\boldsymbol{F}_\lambda = 10^{0.4(C_\lambda - m_\lambda)}$, where the scale factors C_λ are adopted from Heber et al. (1984) for the Strömgren *uvby* filters, and from Johnson (1966) for the infrared *RIJHK* filters.

4. Energy distribution analysis

In order to make a reliable measurement of the atmospheric parameters of sdB stars, it is necessary to deconvolve the hot star flux from that of any cool companion which may be present.

Supposing that binary sdB stars are composed of a hot B-type star and a cool main-sequence or sub-giant star, theoretical flux distributions of both components of the system with a given temperature and gravity can be calculated using appropriate model atmospheres.

In the case of a single sdB star, this model was computed for a given effective temperature $T_{\rm eff}$, surface gravity $\log g$, and angular diameter θ. In the case of a binary system the model was characterized by the effective temperatures, surface gravities and angular diameters of both individual components of the binary system, ($T_{\rm eff}{}^{\rm sdB}$, $T_{\rm eff}{}^{\rm cool}$, $\log g_{\rm sdB}$, $\log g_{\rm cool}$ and $\theta_{\rm sdB}$, $\theta_{\rm cool}$), together with a given chemical composition, metallicity and interstellar extinction A_λ. The latter was characterized by the coefficient E_{B-V} together with the galactic reddening laws of Seaton (1979) and Howarth (1983).

A grid of high-gravity helium-deficient model atmospheres (O'Donoghue et al. 1997) was used to represent the spectrum of the sdB star. This grid of line-blanketed LTE-model atmospheres accounts for the known helium depletion in the atmospheres of B subdwarfs while maintaining solar metallicity. NLTE effects can be neglected for effective temperatures below 35 000 K (Kudritzki 1979). This grid of synthetic spectra covers the effective temperature range 20 000 to 40 000 K (with a spacing of 2000 K), surface gravities range 5.0 to 7.0 dex (with a spacing of 0.5 dex in $\log g$), and 0.0 to 0.3 in He abundance (with a spacing of 0.1 in $n_{\rm He}$).

LTE line-blanketed plane-parallel Kurucz (1993) model atmospheres were used to represent the cool companion on the binary system. This grid of models was selected with surface gravities $\log g = 4.5$ and effective temperatures from 3500 to 18 000 K (with a spacing of 250 K), having the same metallicity as the hot subdwarf flux distributions.

Model fits were performed for each of the values of composition and surface gravity for which models were available, and the best result adopted, i.e., no interpolation in these parameters was attempted.

The physical parameters of the sdB in our sample were obtained by fitting the observed fluxes F_λ with a theoretical flux distribution of the form:

$$\phi_{\lambda,E_{B-V},T_{\rm eff},\theta} = \theta^2 \ \boldsymbol{F}_\lambda(T_{\rm eff}) A_\lambda(E_{B-V}) \quad (1)$$

where $\boldsymbol{F}_\lambda(T_{\rm eff})$ is the absolute monochromatic flux in ergs cm^{-2} s^{-1} Å^{-1} emitted at the stellar surface. In the case of binary stars, Eq. (1) becomes:

$$\phi_\lambda = \left(\theta^2_{\rm sdB} \ \boldsymbol{F}^{\rm sdB}_\lambda(T_{\rm eff}) + \theta^2_{\rm cool} \ \boldsymbol{F}^{\rm cool}_\lambda(T_{\rm eff})\right) \times A_\lambda(E_{B-V}). \quad (2)$$

In the UV, the IUE spectra were rebinned at the sampling resolution of the model atmospheres, while in the optical and infrared each model was binned to the same wavelength bins as the observed photometry. The difference between model and observation was formed to provide the χ^2 statistic:

$$\chi^2 = \sum_\lambda \frac{(F_\lambda - \phi_\lambda)^2}{\sigma^2_\lambda}, \quad (3)$$

where σ^2_λ are the variances of the fluxes within each wavelength bin.

To locate the minimum in the χ^2 surface we used a version of AMOEBA, which performs a multidimensional minimization, by the "*downhill simplex*" method of Nelder & Mead (1965). The implementation of the method is an extension to binary stars of that described by Jeffery et al. (2000) in a study of the UV flux variability of hydrogen-deficient stars.

Together with the grids of hot and cool model atmospheres, the χ^2-minimization needs initial estimates of $T_{\rm eff}, \theta$ and E_{B-V}. In very particular cases, the nature of the χ^2 surface makes extremely important the definition of those initial parameters, since AMOEBA can get stuck in a false minimum. We also define the maximum step that AMOEBA can take, and whether a single parameter can vary or remain fixed during the search.

It is well known that the effective temperature dependence of emergent monochromatic fluxes varies as a function of wavelength (Blackwell & Shallis 1977). Specifically, in determining the angular diameter of a star it is essential to minimise the error in this quantity, which can be directly attributable to an uncertain effective temperature; preferably, that means normalising using an infrared flux which is well down the Rayleigh-Jeans tail and not too close to the 2200 Å feature. For hot stars, where the maximum of the Planck function is close to 1000 Å, the V-band flux is an acceptable choice. Hence, the normalization of observed and model fluxes has been performed at the V-band (5500 Å) by assigning a high weight to the photometric data at this wavelength.

5. Atmospheric parameters determination

The fitting procedures outlined in the previous section were applied to all 34 stars in our sample, assuming first that the star was single and second that it was binary. For a single star both single and binary solutions should give the same result for the sdB star while the binary solution will give a nonsense result for the hypothetical cool star. On the other hand, a binary star will yield quite different single and binary star solutions and the single star solution will not match the observed fluxes at all wavelengths.

On the basis of these comparisons, the initial sample was divided into two groups comprising 15 single sdB stars and 19 binaries containing an sdB star and a cool companion.

Table 3 shows the results of the best fits in the case that the sdB stars energy distribution represents a single star. Columns 1 and 2 give the star identifiers, Cols. 3, 4 and 5 give the adopted surface gravity, interstellar extinction and atmospheric helium abundances, respectively. Column 6 gives the integrated IUE flux, $F_{\rm IUE} = \int_{1150}^{3200} F_\lambda {\rm d}\lambda$, and its standard deviation, $(\int_{1150}^{3200} \sigma^2_\lambda {\rm d}\lambda)^{\frac{1}{2}}$. Column 7 gives the effective temperature and standard error, and Col. 8 gives the angular radius for each spectrum. Table 4 presents the results of the best fits in the case that the energy distribution of the observed sdB star represents a binary system containing a hot subdwarf and a cool companion.

Figure 1 presents the best fits of our UV–optical–infrared observations to theoretical models representing a single subdwarf B star (left panel) and a composite system (right panel), containing a hot subdwarf and a cool companion.

In Fig. 2 we show the detailed fit of the composite sdB *PG 0749+658*, where the theoretical model characterizing the system (solid line) is the combination of a model representing a hot star (dash-dotted line) and a model representing a cool star (dashed line). It is easy to see that the presence of a cool companion in the system produces a flattened continuum in the redder wavelengths range due to the introduced infrared excess. In this way, the slope of the theoretical model atmospheres representing a composite system is flatter than the slope of a model representing a single star. In the case of the sdB *PG 0856+121* (No. 11), the slope of the theoretical model atmospheres representing the system is higher compared with the rest of the composite systems of the sample. The contribution of the cool component in *PG 0856+121* is smaller than in the other cases, explained by the fact that its cool companion has the lowest effective temperature of the sample.

Table 3. Atmospheric parameters of the sdB stars of our sample with flux distributions behaving as a single star. The error of the surface gravity is assumed to be 0.2 dex, with 0.01 assumed for the interstellar extinction and 0.01 for the helium abundance. Solar metallicity is adopted

	Star	$\log g$	$E(B-V)$	$n_{\rm He}$	$F_{\rm IUE}$ (ergs cm^{-2} s^{-1})	$T_{\rm eff}$ (K)	θ (rad)
					$\times 10^{-10}$		$\times 10^{-12}$
1	PG 0004+133	5.0	0.20	0.0	3.310 ± 0.008	$25\,025 \pm 400$	11.100 ± 0.040
4	PG 0229+064	6.0	0.11	0.0	6.380 ± 0.054	$20\,100 \pm 275$	19.700 ± 0.086
6	PG 0240+046	5.5	0.06	0.3	4.180 ± 0.009	$34\,800 \pm 1850$	4.000 ± 0.028
7	PG 0314+146	6.0	0.00	0.0	7.300 ± 0.025	$20\,800 \pm 500$	12.600 ± 0.042
8	PG 0342+026	6.0	0.15	0.0	36.500 ± 0.093	$27\,900 \pm 975$	25.300 ± 0.122
10	PG 0839+399	6.0	0.02	0.0	4.390 ± 0.015	$35\,450 \pm 1800$	3.360 ± 0.036
13	PG 0934+186	6.0	0.00	0.0	12.900 ± 0.018	$31\,000 \pm 6575$	6.560 ± 0.035
15	PG 1047+003	6.0	0.02	0.2	9.450 ± 0.022	$33\,500 \pm 1550$	5.360 ± 0.035
18	PG 1230+052	6.0	0.02	0.0	8.790 ± 0.021	$27\,975 \pm 900$	7.130 ± 0.037
19	PG 1233+426	5.0	0.03	0.0	26.900 ± 0.093	$28\,775 \pm 900$	12.200 ± 0.078
20	PG 1336 -018	6.0	0.02	0.1	8.760 ± 0.021	$29\,825 \pm 900$	6.090 ± 0.029
21	PG 1432+004	5.5	0.07	0.0	9.330 ± 0.024	$25\,500 \pm 700$	10.500 ± 0.048
22	PG 1433+239	6.0	0.05	0.0	15.500 ± 0.035	$26\,750 \pm 780$	11.400 ± 0.066
24	PG 1452+198	6.0	0.02	0.0	19.000 ± 0.047	$28\,025 \pm 7475$	10.300 ± 0.055
34	PG 2259+134	5.5	0.10	0.2	1.820 ± 0.005	$28\,300 \pm 725$	4.260 ± 0.015

Table 4. Atmospheric parameters of sdB stars in which the energy distributions has been modelled as a hot sdB star plus a cool companion. Errors on the surface gravity, interstellar extinction and helium abundance are assumed as in Table 3. Solar metallicity is also adopted

	Star	$\log g^{\rm sdB}$	$E(B-V)$	$n_{\rm He}$	$F_{\rm IUE}$ (ergs cm^{-2} s^{-1})	${T_{\rm eff}}^{\rm sdB}$ (K)	${T_{\rm eff}}^{\rm cool}$ (K)	$\theta_{\rm sdB}$ (rad)	$\theta_{\rm cool}$ (rad)
					$\times 10^{-10}$			$\times 10^{-12}$	$\times 10^{-11}$
2	PG 0105+276	6.0	0.01	0.0	2.290 ± 0.010	$35\,850 \pm 980$	$5\,450 \pm 200$	2.620 ± 0.099	1.660 ± 0.050
3	PG 0110+262	6.0	0.00	0.0	3.520 ± 0.018	$21\,050 \pm 575$	$5\,485 \pm 200$	8.380 ± 0.233	3.510 ± 0.095
5	PG 0232+095	6.0	0.10	0.0	3.670 ± 0.014	$21\,500 \pm 500$	$4\,575 \pm 50$	10.200 ± 0.130	9.050 ± 0.202
9	PG 0749+658	6.0	0.00	0.0	17.500 ± 0.054	$25\,050 \pm 675$	$5\,600 \pm 300$	11.000 ± 0.200	4.250 ± 0.312
11	PG 0856+121	5.5	0.02	0.0	6.340 ± 0.013	$25\,525 \pm 2345$	$3\,625 \pm 1265$	6.960 ± 0.046	1.020 ± 0.438
12	PG 0900+400	5.0	0.00	0.0	6.310 ± 0.020	$25\,000 \pm 925$	$5\,150 \pm 130$	6.970 ± 0.096	5.210 ± 0.118
14	PG 1040+234	6.0	0.02	0.0	2.790 ± 0.016	$23\,275 \pm 675$	$5\,250 \pm 135$	6.510 ± 0.214	3.270 ± 0.089
16	PG 1049+013	5.0	0.00	0.1	0.887 ± 0.005	$18\,600 \pm 700$	$4\,500 \pm 800$	5.630 ± 0.213	2.030 ± 0.259
17	PG 1104+243	5.0	0.00	0.0	35.800 ± 0.097	$28\,000 \pm 875$	$5\,735 \pm 150$	12.800 ± 0.206	7.780 ± 0.190
23	PG 1449+653	5.5	0.02	0.0	4.340 ± 0.018	$28\,150 \pm 9000$	$4\,700 \pm 1475$	5.600 ± 0.181	2.790 ± 0.306
25	PG 1629+081	5.5	0.00	0.0	13.00 ± 0.033	$26\,400 \pm 1150$	$3\,825 \pm 575$	9.040 ± 0.108	3.400 ± 0.773
26	PG 1701+359	6.0	0.00	0.1	9.960 ± 0.020	$36\,075 \pm 700$	$6\,450 \pm 230$	4.450 ± 0.081	2.120 ± 0.064
27	PG 1718+519	6.0	0.01	0.0	3.130 ± 0.015	$29\,950 \pm 1100$	$5\,925 \pm 70$	3.370 ± 0.086	2.770 ± 0.061
28	BD+29° 3070	6.0	0.00	0.0	39.400 ± 0.087	$32\,850 \pm 2750$	$8\,050 \pm 400$	9.860 ± 0.249	9.460 ± 0.105
29	PG 2110+127	7.0	0.03	0.0	4.150 ± 0.022	$24\,900 \pm 6500$	$5\,500 \pm 575$	7.190 ± 0.281	3.950 ± 0.099
30	PG 2135+045	5.5	0.03	0.0	1.400 ± 0.007	$26\,325 \pm 9950$	$4\,375 \pm 1790$	3.830 ± 0.109	1.800 ± 0.236
31	PG 2148+095	6.0	0.00	0.0	5.010 ± 0.023	$22\,950 \pm 825$	$4\,375 \pm 200$	8.500 ± 0.181	4.270 ± 0.142
32	PG 2214+184	5.0	0.00	0.2	0.583 ± 0.004	$15\,200 \pm 450$	$4\,825 \pm 1825$	7.080 ± 0.330	0.894 ± 0.484
33	PG 2226+094	6.0	0.00	0.0	1.240 ± 0.010	$19\,025 \pm 260$	$3\,800 \pm 160$	6.330 ± 0.111	3.980 ± 0.296

The IUE spectra were rebinned at the sampling resolution of the model atmospheres. Error bars are asymmetric because of the logarithmic scale. In cases where $\sigma_\lambda > \boldsymbol{F}_\lambda$, the lower error is set to $\boldsymbol{F}_\lambda/10$. This is the case around Lyman α in stars such as *PG 0229+064* (No. 4), *PG 2214+184* (No. 32) and *PG 2226+096* (No. 33), and in LWR/P spectra such as *PG 0232+095* (No. 5) and *PG 2259+134* (No. 34).

The absence of any photometric data at wavelengths longer than 5500 Å precludes a stringent limit in the determination of atmospheric parameters and the detection of a possible cool companion to some sdBs. This is the case for *PG 0240+046* (No. 6) and *PG 0314+146* (No. 7).

5.1. Error estimations

In the case of a single subdwarf B star, the observed energy distribution is a function of several parameters, i.e., $F_\lambda = f(T_{\rm eff}, \log g, E_{B-V}, n_{\rm He}, Z)$. For a composite system, the flux distribution depends on the parameters of the hot subdwarf and the cool component: $F_\lambda = f({T_{\rm eff}}^{\rm sdB}, {T_{\rm eff}}^{\rm cool}, \log {g}^{\rm sdB}, \log {g}^{\rm cool}, E_{B-V}, n_{\rm He}, Z)$.

In our multi-dimensional fitting procedure, the solution of the system will be more or less sensitive to the initial estimates of some particular atmospheric parameter.

The internal errors associated with the best set of atmospheric parameters, provided by the χ^2-minimization procedure, are given by the diagonal elements $(\alpha^{-1})_{ii}$ of the inverse of the covariance matrix α.

During our χ^2-minimization procedure some parameters are not allowed to vary, i.e., $\log g$, $n_{\rm He}$ and, in some cases, E_{B-V}. For those parameters we make some assumptions for their standard errors. We assume to be 0.2 dex the standard error of the surface gravity, 0.01 is assumed for the interstellar extinction and 0.01 for the helium abundance. The effective temperature is

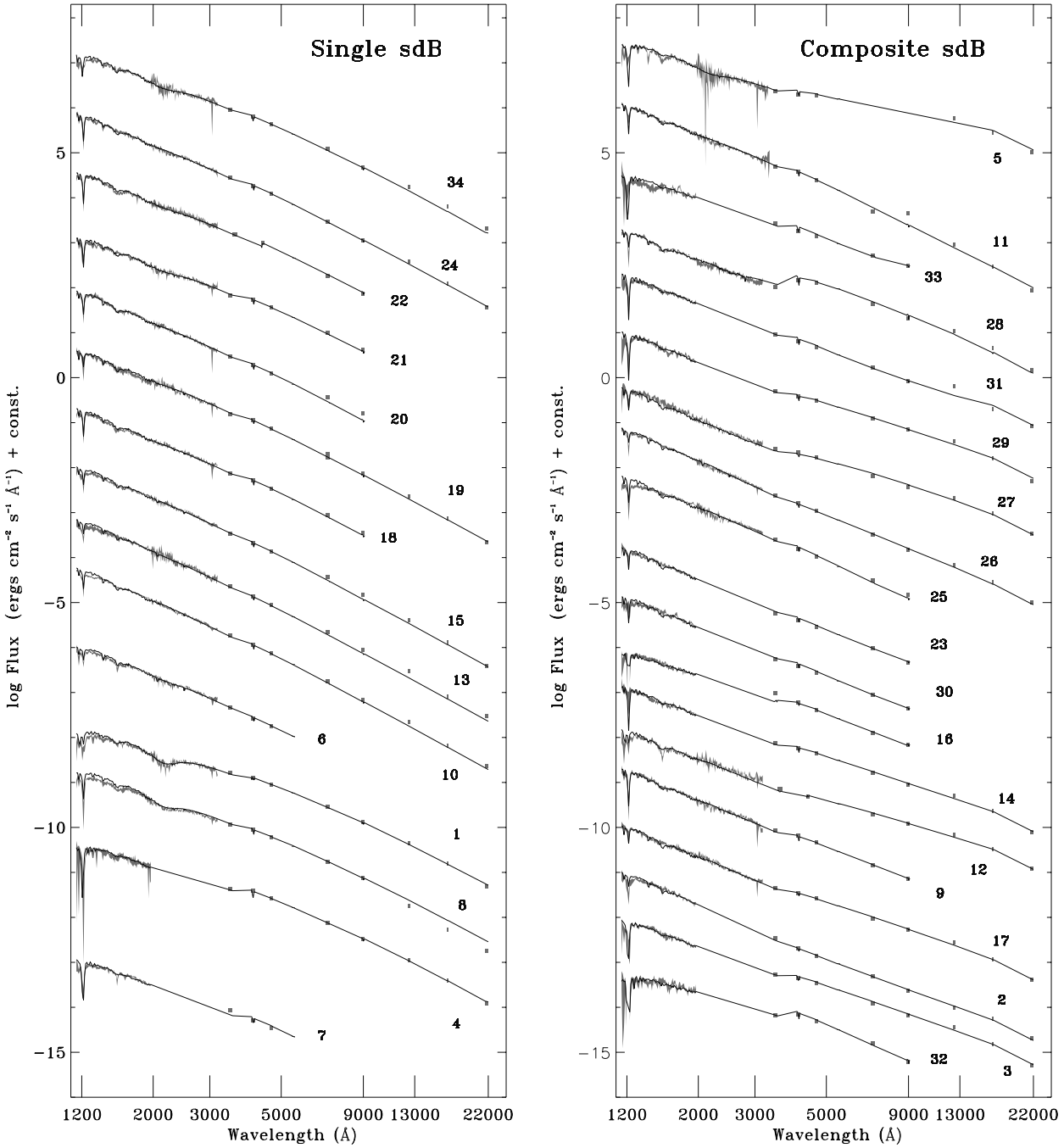

Fig. 1. Best fits of UV–optical–infrared observations to theoretical models representing a single subdwarf B star (left) and a composite system (right) are shown. The light shading represents the IUE spectrum of the star with the data plotted as error bars (the IUE spectrum is composed by a SW spectrum, 1150–1980 Å, and a LW spectrum, 1850–3350 Å), and the standard deviation of the flux in each photometric band (Strömgren *uvby* and infrared Johnson *RIJHK*). The theoretical model atmospheres from the best fit with the observational data is represented by a solid line spectrum. Labels refer to the identification number in Table 1

a variable parameter inside the procedure, i.e., its result will depend on the initial estimates of the fixed parameters, so its standard error must be calculated. On the other hand, the angular radius of the star is a parameter directly linked to the effective temperature and the total flux of the spectrum, $F_\lambda = \theta^2 {T_{\rm eff}}^4$, and its standard error can be considered the one obtained from the χ^2-minimization procedure.

Model fits for values of $\log g = \pm 0.5$ either side of the optimum value were also performed and the difference in the $T_{\rm eff}$ value derived were used to calculate the additional uncertainty in $T_{\rm eff}$ due to an assumed error of ± 0.2 dex in g. The same procedure was followed for E_{B-V} for an assumed error of ± 0.01 and $n_{\rm He}$ for an assumed error of ± 0.1. The total uncertainty given in Tables 3 and 4 is the square root of the sum of the squares of these additional

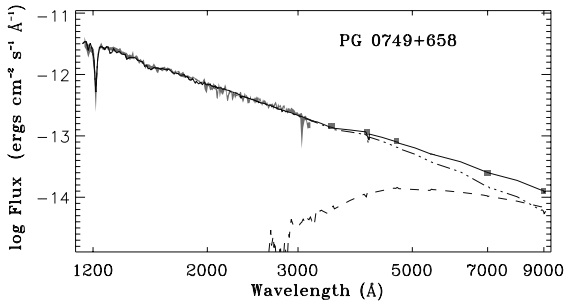

Fig. 2. Detailed fit of the composite system *PG 0749+658*. The light shading represents the IUE spectrum (1150–3350 Å) with the data plotted as error bars, and the standard deviation of the flux in the Strömgren *uvby* and near–infrared Johnson *RI* photometric bands. The theoretical model characterizing the system (solid line) is the combination of a model representing a hot star (dash-dotted line) and a model representing a cool star (dashed line)

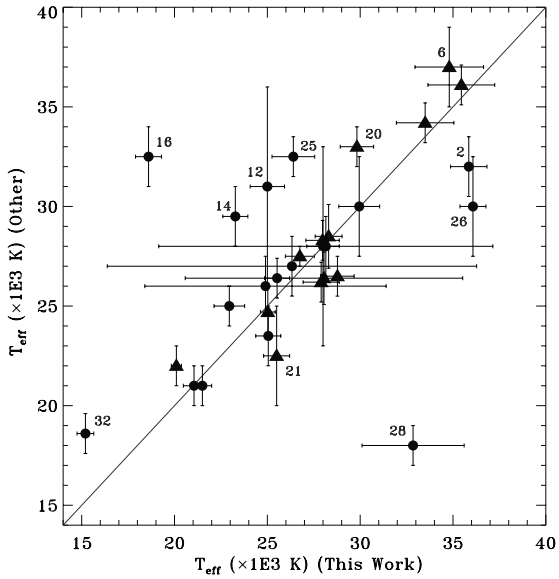

Fig. 3. Comparison between effective temperatures obtained in previous works and with our method, in the case of single sdB stars (filled triangles) and hot components of composite systems (filled circles). The diagonal solid line represents perfect agreement between $T_{\rm eff}$ measurements. Labelled points refer to the identification numbers in Table 1

uncertainties plus the formal error from the χ^2 fitting, i.e.,

$$\sigma^2_{T_{\rm eff}} = \delta^2_{T_{\rm eff}} + \left(\frac{\partial T_{\rm eff}}{\partial E_{B-V}}\right)^2 \delta^2_{E_{B-V}} + \left(\frac{\partial T_{\rm eff}}{\partial \log g}\right)^2 \delta^2_{\log\, g} + \left(\frac{\partial T_{\rm eff}}{\partial\, n_{\rm He}}\right)^2 \delta^2_{n_{\rm He}}. \quad (4)$$

On some occasions, where the part of the IUE spectrum of the star from 1850–3350 Å (LW spectrum) is not available, much larger variations of effective temperature, particularly in the hot component, are found when determining the influence of the fixed parameters in our χ^2-minimization procedure. These are the cases of the composite sdB stars, *PG 1449+653* (No. 23), *PG 2110+127* (No. 29) and *PG 2135+045* (No. 30).

6. Comparison with other analyses

Several other attempts have been made to determine the atmospheric parameters of sdB stars, many in a similar way to that described here.

For example, $T_{\rm eff}$ is estimated either from an analysis of the ultraviolet energy distribution and from intermediate or narrow band photometry (Lamontagne et al. 1987), or by using reddening free colour indices (Theissen et al. 1993). A Balmer line profile then provides the surface gravity. Finally, the equivalent width of a strong helium line gives an estimate of the helium abundance (Möehler et al. 1990; Saffer et al. 1994). The flux-ratio diagram (hereafter FRD) method (Wade 1982) has been used to derive approximate $T_{\rm eff}$ and spectral types of the components of binary sdB stars (Allard et al. 1994). By fitting line-blanketed Kurucz model spectra and ultraviolet, optical and IR fluxes Ulla & Thejll (1998) were able to determine estimates of $T_{\rm eff}$ and relative radii of the two components of composite sdB stars.

The atmospheric parameters of sdB stars overlapping our sample have been gathered from the literature in Table 5. A comparative analysis has been performed between the results obtained with our χ^2-minimization procedure and those obtained in previous works. Note that in some occasions several estimations of $T_{\rm eff}$ have been performed by different authors. In Table 5, the last column showing the reference for each cited measurement has an asterisk whenever these values have been used in our comparative analysis.

Figure 3 shows the effective temperatures of sdB stars obtained by previous authors compared with those obtained with our χ^2-minimization procedure. Each point of the plot represents the measurements of $T_{\rm eff}$ for a single sdB star (filled triangles) or for the hot component of a composite sdB stars (filled circles). The vertical error bars correspond to the standard error of the measurements obtained from previous work, while the horizontal error bars show the uncertainty in the calculation of the $T_{\rm eff}$ using our procedure. In a perfect agreement between results obtained with our method and previous works, all the points within its error bars should stand over the diagonal solid line. The agreement with previous $T_{\rm eff}$ measurements is shown to be satisfactory for most of the targets. Stars with the worst agreement between $T_{\rm eff}$ measurements have been labeled in the plot with their identification number. All our single sdB stars lie within the temperature range $20\,000 < T_{\rm eff}/\,{\rm K} < 36\,000$, while the hot components of binary sdB stars appear to have temperatures within the interval $15\,000 < T_{\rm eff}/\,{\rm K} < 36\,000$.

Figure 4 shows the effective temperatures of the cool companions in binary sdB stars obtained by previous authors compared with those obtained with our χ^2-minimization procedure. The majority of the cool components of our sample of binary sdB stars have

Table 5. Determinations of physical parameters of sdB stars collected from previous works. Ref.: A94 = Allard et al. (1994); F84 = Ferguson et al. (1984); H99 = Heber et al. (1999); K98 = Kilkenny et al. (1998); L85 = Lamontagne et al. (1985); L87 = Lamontagne et al. (1987); M90 = Möehler et al. (1990); O98 = O'Donoghue et al. (1998); S94 = Saffer et al. (1994); Th93 = Theissen et al. (1993); Th95 = Theissen et al. (1995); Tj94 = Thejll et al. (1994); U98 = Ulla & Thejll (1998); W93 = Wood et al. (1993)

	Object	Previous measurements					Ref
		$T_{\rm eff}{}^{\rm sdB}$ (K)	$T_{\rm eff}{}^{\rm cool}$ (K)	$\log g^{\rm sdB}$ (c.g.s)	$\frac{n_{\rm He}}{n_{\rm H}}$	E_{B-V}	
1	PG 0004+133	24 700 ± 1300		4.50 ± 0.20	0.028	0.110	M90⋆
2	PG 0105+276	32 000 ± 1500	3800 ± 500				A94⋆
3	PG 0110+262	22 000 ± 1500	4500 ± 500				A94
		21 000 ± 1000	5000 ± 500	5.90 ± 0.10		0.000	U98⋆
4	PG 0229+064	22 000 ± 1000		4.65 ± 0.15	0.137		S94⋆
5	PG 0232+095	21 000 ± 1000	4750 ± 500	6.60 ± 0.10		0.000	U98⋆
6	PG 0240+046	37 000 ± 2000		5.30 ± 0.30	0.550	0.000	Tj94⋆
8	PG 0342+026	22 300 ± 1000		5.00 ± 0.30		0.100	L87
		24 000 ± 1200		4.90 ± 0.20	0.003	0.080	M90
		26 200 ± 1000		5.67 ± 0.15	0.004		S94⋆
		25 000±2500		5.25±0.20	0.000	0.104	Th95
9	PG 0749+658	23 500 ± 1500	4125 ± 500				A94⋆
		24 600 ± 1000		5.54 ± 0.15	0.004		S94
10	PG 0839+399	36 100 ± 1000		5.91 ± 0.15	0.002		S94⋆
11	PG 0856+121	23 800 ± 1190		5.10 ± 0.20		0.020	M90
		26 400 ± 1000		5.73 ± 0.15	0.001		S94 ⋆
12	PG 0900+400	31 000 ± 5000	4400 ± 1 000				F84⋆
14	PG 1040+234	29 500 ± 1500	4300 ± 500				A94⋆
15	PG 1047+003	34 200 ± 1000		5.60 ± 0.10	0.010		H99⋆
		35 000 ± 1000		5.90 ± 0.10	0.000	0.050	O98
16	PG 1049+013	32 500 ± 1500	3500 ± 500				A94⋆
17	PG 1104+243	28 000 ± 5000	4600 ± 1 000				F84⋆
		27 200 ± 1500		5.50 ± 0.30		0.030	L87
		27 500 ± 1500	4300 ± 500				A94
18	PG 1230+052	28 300 ± 1000		5.72 ± 0.15	0.001		S94⋆
19	PG 1233+426	26 200 ± 1500		5.30 ± 0.30			L85
		26 500 ± 1000		5.60 ± 0.15	0.005		S94⋆
20	PG 1336 -018	32 500 ± 3500	3750				W93
		33 000 ± 1000	3000	6.00 ± 0.10		0.050	K98⋆
21	PG 1432+004	22 400 ± 1120		5.00 ± 0.20	0.005	0.030	M90
		22 500 ± 2500		5.00 ± 0.20	0.000	0.015	Th95⋆
22	PG 1433+239	29 600 ± 1000		5.57 ± 0.15	0.000		S94
		27 500 ± 1000		5.21 ± 0.05			O98⋆
23	PG 1449+653	28 000 ± 1500	4225 ± 500				A94⋆
24	PG 1452+198	26 400 ± 1320		5.00 ± 0.20	0.014	0.000	M90⋆
25	PG 1629+081	32 500 ± 1000					A94⋆
26	PG 1701+359	26 250 ± 1250		5.80 ± 0.20		0.010	Th93
		28 500 ± 1500	4000 ± 500				A94⋆
		30 000 ± 2500		5.00 ± 0.20	0.000	0.015	Th95
27	PG 1718+519	23 500 ± 1000		4.25 ± 0.20		0.010	Th93
		25 000 ± 1500	4300 ± 500				A94
		30 000 ± 2500	5125 ± 500	5.00 ± 0.20	0.000	0.015	Th95⋆
28	BD+29° 3070	18 000 ± 1000	5250 ± 500	5.50 ± 0.10		≤0.030	U98⋆
29	PG 2110+127	25 400 ± 1600		4.20 ± 0.20		0.060	Th93
		26 000 ± 1500	4500 ± 500				A94⋆
		33 700 ± 1000		5.33 ± 0.15	0.004		S94
		30 000 ± 2500	5375 ± 500	5.00 ± 0.20	0.000	0.050	Th95
		34 000 ± 1000	5750	5.90 ± 0.10		0.100	U98
30	PG 2135+045	27 000 ± 1500	4400 ± 500				A94⋆
		32 100 ± 1000		4.79 ± 0.15	0.016		S94
31	PG 2148+095	26 000 ± 1500	4300 ± 500				A94
		25 000 ± 1000	5000 ± 500	5.80 ± 0.10			U98⋆
32	PG 2214+184	18 600 ± 1000		4.26 ± 0.15	0.023		S94⋆
34	PG 2259+134	28 500 ± 1600		5.30 ± 0.20	0.022	0.030	Th93⋆
		22 500 ± 2500		5.00 ± 0.20	0.000	0.015	Th95

temperatures in the range $3\,800 < T_{\rm eff}/\,{\rm K} < 6\,000$, with the exception of *PG 1701+359* (No. 26) and *BD+29° 3070* (No. 28), having approx. 6 500 K and 8 000 K, respectively. Our measurements of $T_{\rm eff}$ of cool companions are mostly higher than those obtained by other authors. Stars with the poorest agreement are labelled in the plot with their identification numbers. We believe that, in general, our use of photometry from the UV to the near–infrared provides a more reliable measure of $T_{\rm eff}$ for both components than, for example, those obtained using the FRD method.

6.1. Stars of particular interest

We briefly comment on those cases in which the largest discrepancies are found between our $T_{\rm eff}$ measurements and those of other authors.

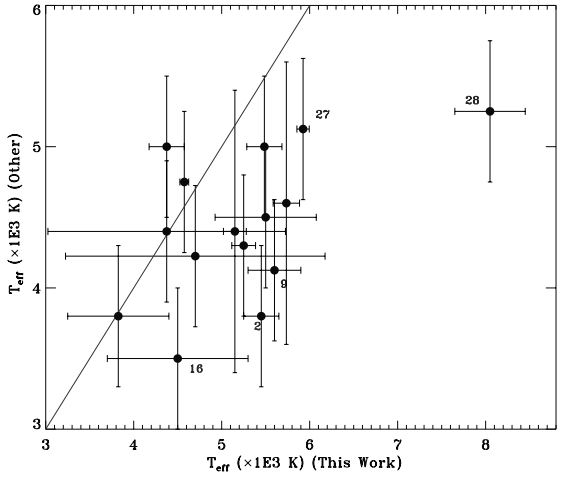

Fig. 4. As Fig. 3 but for the case of cool components in composite sdB stars

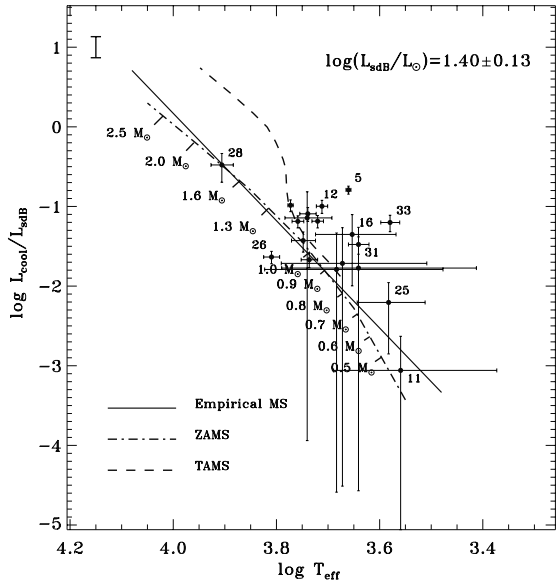

Fig. 5. Positions of the cool stars in composite sdB stars in the (log L–log $T_{\rm eff}$) plane as derived from our data. A typical value of $\log(L_{\rm sdB}/L_{\odot}) = 1.40 \pm 0.13$ is assumed for all sdB stars. Filled circles represent the location of the cool companion of the systems. The position of an empirical Main-sequence is plotted as solid line (Lang 1992), the dash-dotted and dashed lines represent the evolutionary tracks of the ZAMS and TAMS, respectively, for stellar models with solar composition and mass range coverage from 0.25 up to 2.5 $M_{\odot}$ (Girardi et al. 2000). Labelled points refer to the identification numbers in Table 1. Error bar (top left) represents standard error in $L_{\rm sdB}$

PG 0240+046 (No. 6): This single star was classified as a helium-rich subdwarf O star (Thejll et al. 1994), with $n_{\rm He} = 0.55$. Our results agree with this, although the model atmospheres used in our calculations had $n_{\rm He} = 0.3$. Models with higher helium abundances would be needed for a better analysis of this system.

PG 0342+026 (No. 8), *PG 1701+359* (No. 26), *PG 1718+519* (No. 27), *PG 2110+127* (No. 29) and *PG 2259+134* (No. 34): These single and composite systems are another case of interest, for which several authors have measured $T_{\rm eff}$ obtaining quite different values (see Table 5). In the cases of the single *PG 0342+026* and *PG 2259+134* our results are in better agreement with those from Theissen et al. (1993). In the cases of composite *PG 1701+359* and *PG 1718+519*, our measurements of $T_{\rm eff}$ agree better with the results by Theissen et al. (1995). However, for *PG 2110+127* our $T_{\rm eff}$ is in good agreement with those obtained by Allard et al. (1994) and Theissen et al. (1993).

BD+29° 3070 (No. 28): For this particular star a very big disagreement exists between measurements of $T_{\rm eff}$ reported by Ulla & Thejll (1998) and those coming from our analysis. The enhancement of the energy distribution above 4500 Å of the theoretical model atmosphere representing this system demonstrates the presence of a cool companion of high $T_{\rm eff}$. A reddening of $E_{B-V} \leq 0.025$ was assigned by those authors, which is comparable with our estimate $E_{B-V} = 0.00$, so the big difference found in $T_{\rm eff}$ can not be associated with this factor. This particular star has to be verified. The high effective temperature of the cool component obtained with our method would imply an early spectral type (A6) main-sequence star (Lang 1982).

PG 1049+013 (No. 16): A big discrepancy also occurs with the $T_{\rm eff}$ measurements of the hot component of this composite sdB star. Allard et al. (1994) found $T_{\rm eff}{}^{\rm sdB} = 32\,500 \pm 1500$ K while our measurement gives a much lower temperature ($18\,600 \pm 700$ K). The value of u magnitudes used by those authors in their work leads to a very high $T_{\rm eff}$ for the hot subdwarf. However, in our analysis the trend of the IUE spectrum of *PG 1049+013* implies the presence of a much cooler sdB component.

PG 0900+400 (No. 12) and *PG 1104+243* (No. 17): The large uncertainties in the measurement of $T_{\rm eff}$ by Ferguson et al. (1984) on the hot components of these systems ($\pm 5\,000$ K) makes our measurements consistent with those of those authors. The FRD method has been used by those authors for obtaining the spectral types of the cool companions of these systems. Thus, such large errors in the determination of $T_{\rm eff}$ on these two hot subdwarfs will lead to large uncertainties in the determination of $T_{\rm eff}$ on their cool companions (± 1000 K has been adopted).

7. Hertzsprung-Russell diagram

The determination of effective temperatures and surface gravities of sdB stars is of special interest for understanding the evolution of hot subdwarf stars. In view of our results obtained for the physical parameters of sdB stars, it is worthwhile to check the interpretation of the evolutionary status of both components of the binary systems of our sample.

A modified Hertzsprung-Russell (Luminosity–Effective temperature) diagram can be built up to locate the approximate positions of the cool components of our binary systems, with the parameters derived from our method.

Figure 5 shows the location of the cool stars in composite sdB of our sample within the Hertzsprung-Russell ($\log(L_{\rm cool}/L_{\rm sdB})$–$\log\ T_{\rm eff}$) diagram. The surface luminosity ratio used in this plot has been calculated with the parameters derived from our method as follow:

$$\left(\frac{L_{\rm cool}}{L_{\rm sdB}}\right) = \left(\frac{\theta_{\rm cool}}{\theta_{\rm sdB}}\right)^2 \left(\frac{{T_{\rm eff}}^{\rm cool}}{{T_{\rm eff}}^{\rm sdB}}\right)^4 . \quad (5)$$

Adopting a typical value of $\log(L_{\rm sdB}/L_\odot) = 1.4 \pm 0.13$ (Möehler et al. 1997) for the hot subdwarf stars, based on a study of hot Horizontal Branch stars in globular clusters, the position of an empirical main-sequence (Lang 1992) is plotted with a solid line. The evolutionary tracks of the zero age main-sequence (ZAMS) and the terminal age main-sequence (TAMS), appearing as dash-dotted and dashed lines, respectively, have been adopted from stellar models with solar composition, i.e. $[Z = 0.019, Y = 0.273]$ and masses from 0.25 to 2.5 $M_\odot$ (Girardi et al. 2000). These theoretical models were computed using the classical Scwarzschild criterion for convective boundaries (i.e., without overshooting). In the case of stellar masses lower than 0.6 $M_\odot$, the main sequence evolution takes place on time scales much larger than a Hubble time.

The majority of the cool companions lie close to the main sequence with luminosities within 0.5 dex of the assumed ZAMS. Four stars, *PG 0900+400* (No. 12), *PG 1049+013* (No. 16), *PG 1629+081* (No. 25) and *PG 2148+095* (No. 31), lie between 0.5 and 1.0 dex above the assumed ZAMS; these are also consistent with main-sequence luminosities given the anticipated error in $L_{\rm sdB}$. Two stars, *PG 0232+095* (No. 5) and *PG 2226+094* (No. 33), have luminosities >1 dex above the ZAMS and appear to have evolved away from the main sequence. Furthermore, one star, *PG 1701+359* (No. 26), appears to be subluminous, being 0.5 dex below the assumed ZAMS.

Due to the uncertainty in our assumption of the surface luminosity of sdB stars, the effective temperature is the major parameter of constraint in our HR diagram. The large majority of the cool stars in composite sdB are in the range of $T_{\rm eff}$ $4000 < {T_{\rm eff}}^{\rm cool}/\,{\rm K} < 6000$. According to these effective temperatures, they are consistent with main-sequence stars of masses between $0.8 < M_{\rm cool}/M_\odot < 1.3$, with the exception of *BD+29° 3070* (No. 28) (about 1.8 $M_\odot$), and the very low-mass stars *PG 0856+121* (No. 11) and *PG 1629+081* (No. 25), about 0.4 $M_\odot$ and 0.65 $M_\odot$, respectively.

With our results and assumption on subdwarf B surface luminosity, we can conclude that the majority of the cool components of our sample of binary sdB stars are main-sequence stars.

8. Discussion

The fact that there is no spectrophotometric evidence for a cool companion in an observed sdB star does not mean that a cool companion is not present but, perhaps, only that is not detectable with a particular method. Thus, it is important to estimate lower limits on detectability of companions of possible binary systems.

In order to determine the coolest main sequence stars detectable with our method, we constructed a series of test spectra for composite systems having relative radii comparable to those of sdB and MS stars, and with a range of $T_{\rm eff}$ for both stars. We found that for all sdB temperatures $T_{\rm eff} > 26\,000$ K, all MS companions with $T_{\rm eff} > 3500$ K were recovered if the hot star parameters were fixed in the fit. Relaxing this condition, we always recovered MS stars with $T_{\rm eff} > 4250$ K. For cooler test companions, we consistently recovered $T_{\rm eff} \sim 4250$ K, but the angular radii were always reduced in such a way that total flux was conserved. Consequently, for the coolest companions $T_{\rm eff} \lesssim 4250$ K, there is a systematic tendency to overestimate $T_{\rm eff}$ but *not* $L_{\rm cool}/L_{\rm sdB}$. This affects those stars in our sample which are already furthest from the main-sequence (Fig. 5). It does not affect our conclusion that the majority of companions in our sample are main sequence stars, nor does it affect the luminosity function (Fig. 6).

If the sample of sdB stars were truly representative and the distribution of sdB companions representative of low-mass stars in the field, the fraction of binary sdB stars might then be estimated from a suitable luminosity function (e.g. Lang 1980).

Our sample of 19 cool companions of composite sdB stars are in the range of absolute visual magnitudes $2.59 < M_{\rm v} < 10.70$, 11 of these being main-sequence stars between the interval $4 < M_{\rm v} < 6$.

With these absolute visual magnitudes an histogram has been built (Fig. 6) where the number of objects, in bins of $\delta M_{\rm v} = 2$, are represented. Thus, assuming that the luminosity function of the secondary stars of our composite sdB can be represented by that of single stars of luminosity class V, the main-sequence luminosity function by Lang (1980) (hereafter LF80) has been normalized to the interval $4 < M_{\rm v} < 6$, and integrated over all the range of $M_{\rm v}$ within which binary systems are detectable with our method. In Fig. 6 filled circles represent this luminosity function binned with the same resolution as our histogram. Poisson statistics have been used to estimate the standard errors of the luminosity function per interval of $M_{\rm v}$.

The fact that only five composite sdB stars have been observed beyond $M_{\rm v} = 6$ means that, either there are no M dwarf companions among sdB stars, or that strong selection effects are present in our sample. Extending LF80 to the range $6 < M_{\rm v} < 10$, we would expect to observe ∼8 cool companions in the interval $6 < M_{\rm v} < 8$, ∼11 secondary components of composite sdB within $8 < M_{\rm v} < 10$ and ∼19 within $10 < M_{\rm v} < 12$. Although a larger sample of composite sdB stars is required, there already appears to be a shortfall of cool sdB companions with $M_{\rm v} > 6$. Indeed, if sdB stars follow the main-sequence luminosity function, given the shape of the LF for $M_{\rm v} > 12$ (Gould et al. 1997), then *all of our sample should be binaries with cool unseen companions!*

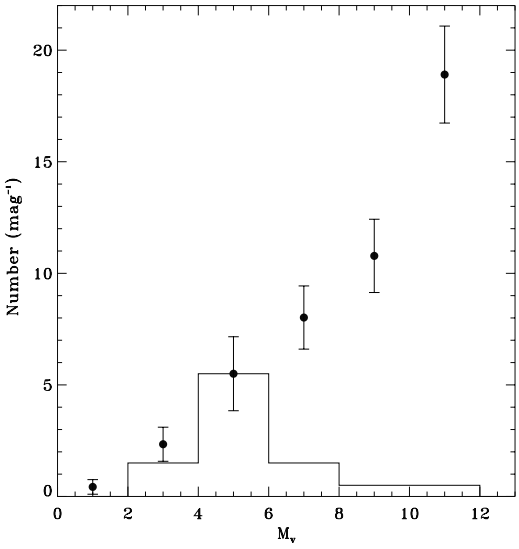

Fig. 6. Histogram representing the number of cool companions in composite sdB stars used in this work, per magnitude, at different absolute visual magnitudes, M_v. The histogram has been performed binning over two M_v. Filled circles represent the main-sequence luminosity function from Lang (1980) normalized to the interval $4 < M_v < 6$, and integrated over the range of M_v of our sample. Poisson statistics have been used to estimate the standard errors of the luminosity function

However, the selection criterion for our sample is that the target was observed with IUE. This implies a complicated mix of selection effects imposed by the original observing programmes – bright, single, composite, peculiar, etc. The principal problem is the absence of companions with $6 < M_v < 8$, since the detection at $M_v > 8$ may be spurious. The deficit is $\sim$2 mag^{-1} detected versus $\sim$8 mag^{-1} predicted from the LF.

Thus, we can only place limits on the sdB binary fraction of between $\sim$56%, based on the shortfall of sdB companions with $M_v > 6$, actually detected, and 100% assuming a standard LF for main-sequence stars. We cannot yet establish that this binary fraction is fundamentally different to that for the supposed progenitor stars. The fraction of F/G main sequence stars which have companions is $\sim$67% (Duquennoy & Mayor 1991).

In general, the effective temperatures of the cool companions of composite sdB stars obtained with our method are systematically higher than those measured by other authors. If $T_{\rm eff}$ of the cool star is reduced, its radius must increase in order to conserve the flux due to the cool star in the composite spectrum. Thus, if previous studies are correct, cool companions would have to be more *evolved* than they appear to be here. Thus, we believe that our measurements of $T_{\rm eff}$ are consistent with the majority of cool companions of our sample being main sequence stars. The assumption of $\log g = 4.5$ used in our analysis does not affect the $T_{\rm eff}$ of the companions.

The fact that our $T_{\rm eff}$ measurements of cool companions are higher than those measured by other authors (Ferguson et al. 1984; Allard et al. 1994; Thejll et al. 1995; Ulla & Thejll 1998), makes their absolute visual magnitudes fainter than our own (see Table 6), being $\sim$2 mag brighter than those of Allard et al. (1994). In these studies, the absolute visual magnitudes were deduced from $T_{\rm eff}$ or spectral types assuming the cool components lie on the Population I main sequence tabulated by Allen (1973).

As suggested in Sect. 6.1, the FRD method may mislead the determination of $T_{\rm eff}$. Typical errors in the classification of a star with this method of the order of $\pm$2 subclasses imply a difference of $\sim$1 mag in the calculation of the absolute visual magnitude, M_v.

Table 6. Absolute visual magnitudes of some of the cool components of our sample together with measurements from other authors. ${T_{\rm eff}}^{\rm cool}$ are effective temperatures of cool stars, obtained with our method. A typical value of $\log(L_{\rm sdB}/L_\odot) = 1.40 \pm 0.13$ is assumed for all sdB stars. M_v are the absolute visual magnitudes obtained with our method (BC coefficients adopted from Lang 1992); $M_v^{\rm F}$ from Ferguson et al. (1984); $M_v^{\rm A}$ from Allard et al. (1994); $M_v^{\rm T}$ from Thejll et al. (1995) and $M_v^{\rm U}$ from Ulla & Thejll (1998) (in all previous measurements BC coefficients adopted from Allen 1973)

Object	${T_{\rm eff}}^{\rm cool}$ (K)	M_v (mag)	Previous measurements $M_v^{\rm F}$	$M_v^{\rm A}$	$M_v^{\rm T}$	$M_v^{\rm U}$
2 PG0105+276	5450 ± 200	5.79	—	8.20	—	—
3 PG0110+262	5485 ± 200	4.36	—	6.60	5.10	6.23
5 PG0232+095	4575 ± 50	3.79	—	—	6.30	6.17
9 PG0749+658	5600 ± 300	5.19	—	7.50	—	—
12 PG0900+400	5150 ± 130	4.09	6.70	—	—	–
16 PG1049+013	4500 ± 800	5.24	—	8.70	—	—
17 PG1104+243	5335 ± 90	4.46	6.60	6.90	—	—
23 PG1449+653	4700 ± 1475	6.05	—	7.00	—	—
25 PG1629+081	3825 ± 575	8.19	—	8.20	—	—
26 PG1701+359	6440 ± 500	5.48	—	7.80	—	—
27 PG1718+519	5925 ± 70	3.90	—	6.90	—	—
28 BD+29°3070	8050 ± 400	2.59	—	—	—	5.45
29 PG2110+127	5500 ± 575	4.49	—	6.60	—	4.78
30 PG2135+045	4375 ± 1790	6.38	—	6.70	—	—
31 PG2148+095	4375 ± 200	5.64	—	6.90	—	5.77

9. Conclusions

On the basis of the available optical and infrared photometry, we can conclude that the energy distribution of 15 sdB stars of our sample are consistent with those of a single sdB star, and 19 sdB stars of the sample show evidences of the presence of a cool companion in the system. In the case of single hot subdwarf stars their effective temperatures range between $20\,000 < {T_{\rm eff}}^{\rm sdB}/{\rm K} < 36\,000$. However, hot components of composite sdB stars of our sample have effective temperatures ranging $15\,000 < {T_{\rm eff}}^{\rm sdB}/{\rm K} < 36\,000$. The majority of the cool stars of composite sdBs in our sample are believed to be main-sequence stars with effective temperatures between 3800 K and 6000 K, although two of them, *PG 0232+095* and *PG 2226+094*, seem to be more evolved. Based on their effective temperatures, the majority of the cool stars of our sample have masses in the range $0.8 < M_{\rm cool}/M_\odot < 1.3$.

Our sample of 19 cool companions are in the range of absolute visual magnitudes $2.59 < M_v < 10.70$, 11 of these being main-sequence stars in the interval $4 < M_v < 6$.

The results of this work show that the majority of the cool companions to our sample of sdB stars are main-sequence stars, in contrast to previous results based on data over a shorter wavelength range and obtained using different techniques (Allard et al. 1994; Theissen et al. 1995).

It is not clear whether the cool companions have influenced the evolution of the sdB star or otherwise caused their peculiar properties. However, some of the binaries identified in this work will be close binaries which have interacted, some will be non-interacting pairs and some will be unrelated optical doubles, i.e. background/foreground stars (Sect. 2), which may explain why some cool companions appear under/over-luminous (see Fig. 5).

Acknowledgements. This publication makes use of data products from the Two Micron All Sky Survey, which is a joint project of the University of Massachusetts and the Infrared Processing and Analysis Center/California Institute of Technology, funded by the National Aeronautics and Space Administration and the National Science Foundation.

The authors would like to thank Tony Lynas-Gray for providing the high-gravity helium-deficient model atmospheres used in this work. We thank Ulrich Heber and Sabine Möehler for good comments and useful suggestions in improving this paper. Thanks go also to the anonymous referee for valuable advice.

This research is supported by a grant to the Armagh Observatory from the Northern Ireland Department of Culture, Arts and Leisure.

References

Allard, F., Wesemael, F., Fontaine, G., Bergeron, P., & Lamontagne, R. 1994, AJ, 107, 1565
Allen, C. W. 1973, Astrophysical Quantities, 3rd Ed. (London: Athlone)
Blackwell, D. E., & Shallis, M. J. 1977, MNRAS, 180, 177
Bixler, J. V., Bowyer, S., & Laget, M. 1991, A&A, 250, 370
Cutri, R. M., Skrutskie, M. F., Van Dysk, S., et al. 2000, Explanatory Supplement to the 2MASS Second Incremental Data Release
Duquennoy, A., & Mayor, M. 1991, A&A, 248, 485
Ferguson, D. H., Green, R. F., & Liebert, J. 1984, ApJ, 287, 320
Girardi, L., Bressan, A., Bertelli, G., & Chiosi, C., 2000, A&AS, 141, 371
Gould, A., Bahcall, J. N., & Flynn, C. 1997, ApJ, 482, 913
Heber, U., Hunger, K., Jonas, G., & Kudritzki, R. P. 1984, A&A, 130, 119
Heber, U. 1986, A&A, 155, 33
Heber, U., Edelmann, H., Lemke, M., Napiwotzki, R., & Engels, D. 1999, in 11th European Workshop on White Dwarfs, ASP Conference Series 169, ed. S. E. Solheim, & E. G. Meistas (Astronomical Society of the Pacific), 551
Howarth, I. D. 1983, MNRAS, 203, 301
Iriarte, B. 1959, Lowell Obs. Bull., 4, 130
Jeffery, C. S., Starling, R. L. C., Hill, P. W., & Pollaco, D. L. 2000, MNRAS, in press
Johnson, H. L. 1966, ARA&A, 4, 193
Kilkenny, D., O'Donoghue, D., Koen, C., Lynas-Gray, A. E., & van Wyk, F. 1998, MNRAS, 296, 329
Kudritzki, R. P. 1979, The elements and their isotopes in the universe, 22nd Liége International symp., 295
Kurucz, R. 1993, ATLAS9 Stellar Atmosphere Programs and 2 km s^{-1} grid, Kurucz CD-ROM No. 13, Cambridge, Mass.: Smithsonian Astrophysical Observatory
Lamontagne, R., Wesemael, F., & Fontaine, G. 1985, ApJ, 299, 496
Lamontagne, R., Wesemael, F., & Fontaine, G. 1987, ApJ, 318, 844
Landolt, A. U. 1992, AJ, 104, 340
Lang, K. R. 1980, Astrophysical formulae, 2nd edition (Springer-Berlin)
Lang, K. R. 1992, Astrophysical data: Stars and planets (Springer-Verlag, New York)
Lipunova, N. A., & Shugarov, S. Yu. 1991, IBVS, 3580
Massey, P. 1992, A User's Guide to CCD Reductions with IRAF, NOAO Laboratory
Massey, P., & Davis, L. E. 1992, A User's Guide to Stellar CCD Photometry with IRAF, NOAO Laboratory
Mengel, J. G., Norris, J., & Gross, P. G. 1976, ApJ, 204, 488
Möehler, S., Richtler, T., Boer, K. S., Dettmar, R. J., & Heber, U. 1990, A&AS, 86, 53
Möehler, S., Heber, U., & Rupprecht, G. 1997, A&A, 319, 109
Nelder, J. A., & Mead, R. 1965, Computer J., 7, 308
Nichols, J. S., & Linsky, J. L. 1996, AJ, 111, 517
O'Donoghue, D., Lynas-Gray, A. E., Kilkenny, D., Stobie, R. S., & Koen, C. 1997, MNRAS, 285, 657
O'Donoghue, D., Koen, C., Lynas-Gray, A. E., Kilkenny, D., & van Wyk, F. 1998, MNRAS, 296, 306
Saffer, R. A., Bergeron, P., Koester, D., & Liebert, J. 1994, ApJ, 432, 351
Saffer, R. A., Livio, M., & Yungelson, L. R. 1998, ApJ, 502, 394
Seaton, M. J. 1979, MNRAS, 187, 73
Stetson, P. B. 1991, AJ, 102, 589
Sweigart, A. V. 1997, ApJ, 474, L23
Theissen, A., Möehler, S., Heber, U., & de Boer, K. S. 1993, A&A, 273, 524
Theissen, A., Möehler, S., Heber, U., Schmidt, J. H. K., & de Boer, K. S. 1995, A&A, 298, 577
Thejll, P., Bauer, F., Saffer, R., Liebert, J., Kunze, D., & Shipman, H. L. 1994, ApJ, 433, 819
Thejll, P., Ulla, A., & MacDonald, J. 1995, A&A, 303, 773
Ulla, A., & Thejll, P. 1998, A&AS, 132, 1
Wade, R. A. 1982, AJ, 87, 1558
Wesemael, F., Fontaine, G., Bergeron, P., Lamontagne, R., & Green, R. F. 1992, AJ, 104, 203
Wood, J. H., Zhang, E. H., & Robinson, E. L. 1993, MNRAS, 261, 103